Inorganic Chemistry

Article

pubs.acs.org/IC

Enhanced Vapor-Phase Processing in Fluorinated Fe_4 Single-Molecule Magnets

Luca Rigamonti,[†,‡] Marco Piccioli,[†] Luigi Malavolti,[‡] Lorenzo Poggini,[‡] Matteo Mannini,[‡] Federico Totti,[‡] Brunetto Cortigiani,[‡] Agnese Magnani,[§] Roberta Sessoli,*[,‡] and Andrea Cornia*[,†]

[†]Dipartimento di Scienze Chimiche e Geologiche, Università degli Studi di Modena e Reggio Emilia & INSTM RU of Modena and Reggio Emilia, via G. Campi 183, 41125 Modena, Italy

[‡]Laboratory of Molecular Magnetism (LaMM), Dipartimento di Chimica 'Ugo Schiff', Università degli Studi di Firenze & INSTM RU of Firenze, via della Lastruccia 3-13, 50019 Sesto Fiorentino (FI), Italy

[§]Dipartimento di Biotecnologie, Chimica e Farmacia, Università degli Studi di Siena & INSTM RU of Siena, Via A. Moro 2, 53100 Siena, Italy

Supporting Information

ABSTRACT: A new tetrairon(III) single-molecule magnet with enhanced volatility and processability was obtained by partial fluorination of the ancillary β-diketonato ligands. Fluorinated proligand H*pta* = pivaloyltrifluoroacetone was used to assemble the bis(alkoxido)-bridged dimer $[Fe_2(OEt)_2(pta)_4]$ (**1**) in crystalline form, from which the new tetranuclear complex $[Fe_4(L)_2(pta)_6]$ (**2**) was synthesized in a one-pot reaction with H_3L = 2-hydroxymethyl-2-phenylpropane-1,3-diol, NaOEt, and $FeCl_3$ in a Et_2O:EtOH solvent mixture. The structure of compound **2** was inferred from ^1H NMR, mass spectrometry, magnetic measurements, and DFT calculations. Direct current magnetic data are consistent with the expected metal-centered triangular topology for the iron(III) ions, with an antiferromagnetic coupling constant J = 16.20(6) cm^{-1} between the central iron and the peripheral ones and consequent stabilization of an S = 5 spin ground state. Alternating current (ac) susceptibility measurements in 0 and 1 kOe static applied fields show the presence of a thermally activated process for magnetic relaxation, with $\tau_0 = 2.3(1)\ 10^{-7}$ s and U_{eff}/k_B = 9.9(1) K at zero static field and $\tau_0 = 2.0(2)\ 10^{-7}$ s and U_{eff}/k_B = 13.0(2) K at 1 kOe. At a pressure of 10^{-7} mbar, compound **2** sublimates at (440 ± 5) K vs (500 ± 10) K for the nonfluorinated variant $[Fe_4(L)_2(dpm)_6]$ (H*dpm* = dipivaloylmethane). According to XPS, ToF-SIMS, and ac susceptibility studies, the chemical composition, fragmentation pattern, and slow magnetic relaxation of the pristine material are retained in sublimated samples, suggesting that the molecular structure remains totally unaffected upon vapor-phase processing.

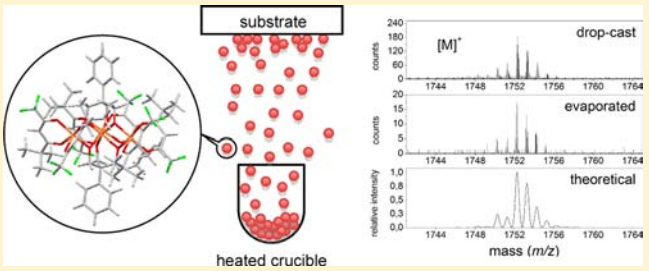

INTRODUCTION

Single-molecule magnets (SMMs) are among the most promising molecular systems featuring low-temperature bistability and quantum behavior.[1] Intense research activity is now devoted both to the design of new, better performing SMMs[2] and to their organization on surfaces,[3,4] with the prospect of utilizing molecular spins to store and process information. In spite of their quite low blocking temperature,[5,6] tetrairon(III) SMMs with a metal-centered triangular topology are offering long-sought opportunities in the field as they display the redox stability, structural robustness,[7] and chemical versatility[8,9] required to build up molecular-based nanodevices.[7] The tripodal ligands which support their structure can be used to promote anchoring on surfaces,[8] a strategy that has recently led to the first observation of magnetic hysteresis and quantum tunneling of the magnetization in gold-wired molecules.[11,12] Most important, the derivative $[Fe_4(L)_2(dpm)_6]$ (H_3L = 2-hydroxymethyl-2-phenylpropane-1,3-diol, H*dpm* = dipivaloylmethane) represents one of the few SMMs that can be thermally evaporated in high vacuum (HV)[13] and the sole example of a polynuclear SMM for which retention of magnetic properties upon sublimation has been demonstrated.[13a] Such a possibility is crucial for assembling SMMs on highly reactive substrates, such as ferromagnetic metals that need to be handled in ultrahigh vacuum (UHV) environments to maintain their surface magnetic properties.[14]

To further facilitate sublimation and improve the possibility to handle this system in UHV, in this work we replaced H*dpm* with pivaloyltrifluoroacetone (H*pta*) in the structure of $[Fe_4(L)_2(dpm)_6]$. Here we report the synthesis and X-ray structure of the intermediate $[Fe_2(OEt)_2(pta)_4]$ (**1**) along with the preparation and chemical, magnetic, and computational characterization of $[Fe_4(L)_2(pta)_6]$ (**2**). Compound **2** not only provides the second example of an evaporable polynuclear SMM but also displays a significantly enhanced volatility as

Received: January 7, 2013
Published: May 9, 2013

   dx.doi.org/10.1021/ic400037c | *Inorg. Chem.* 2013, 52, 5897−5905

compared with $[Fe_4(L)_2(dpm)_6]$ and can be evaporated intact at temperatures as low as (440 ± 5) K at 10^{-7} mbar.

EXPERIMENTAL SECTION

Materials and Methods. All chemicals and solvents were of reagent grade and used as received unless otherwise stated. Ethanol was distilled over magnesium ethoxide and stored over 3 Å molecular sieves. Diethyl ether was predried over $CaCl_2$ overnight and distilled from sodium benzophenone under N_2 before use. Sodium ethoxide was used as a ≅1.5 mol L^{-1} solution in ethanol, freshly prepared by careful addition of sodium metal to anhydrous ethanol under N_2. The tripodal proligand H_3L = 2-hydroxymethyl-2-phenylpropane-1,3-diol was synthesized as outlined in the literature.[15] Elemental analyses were carried out on a Carlo Erba EA1110 CHNS-O automatic analyzer. ^{1}H NMR spectra were recorded with a Bruker FT-DPX200 NMR spectrometer at 200 MHz; chemical shifts δ are given in ppm versus external TMS. Infrared spectra were recorded as KBr disks using a Jasco FTIR-4200 spectrophotometer with a 2 cm^{-1} resolution. MS-MALDI spectra were recorded using an Applied Biosystems/MDS SCIEX 4800 *Plus* MALDI ToF/ToF analyzer equipped with a diode-pumped, solid-state Nd:YAG (355 nm) 200 Hz laser; samples were prepared dissolving the compounds in acetonitrile and using 1,8,9-trihydroxyanthracene as matrix.

Synthesis of $[Fe_2(OEt)_2(pta)_4]$ (1). A pale yellow solution of H*pta* (0.208 g, 1.06 mmol) and NaOEt (1.20 mL of a 1.56 mol L^{-1} solution, 1.87 mmol) in ethanol (2.40 mL) was added dropwise to a stirred solution of $FeCl_3$ (0.0815 g, 0.502 mmol) in ethanol (6.00 mL). During addition a color change from orange to red and back to orange was observed, with concomitant precipitation of NaCl. The mixture was left under stirring at room temperature for 2 h and then filtered, and the white solid was discarded; the resulting solution was left under slow evaporation till formation of orange crystals, suitable for X-ray diffraction, that were collected and dried in vacuo (0.228 g, 92.1%). Melting point: 97−99 °C (without decomposition). Anal. Calcd for $C_{36}H_{50}F_{12}Fe_2O_{10}$ (982.46): C, 44.01; H, 5.13. Found: C, 44.19; H, 5.08. IR (KBr): 2973 ($\nu_{C-H,tBu}$), 2881 ($\nu_{C-H,pta}$), 1624, 1613, 1594 ($\nu_{C=O}$), 1310, 1254, 1197, 1150 (ν_{C-F}), 1039 (ν_{C-O}) cm^{-1}.

Synthesis of $[Fe_4(L)_2(pta)_6]$ (2). Solid $FeCl_3$ (0.0205 g, 0.125 mmol) and NaOEt (240 μL of a 1.45 mol L^{-1} solution in ethanol, 0.349 mmol) were added to a solution of **1** (0.169 g, 0.172 mmol) in Et_2O:EtOH 2:1 (15.0 mL). The orange mixture was stirred for 30 min, diluted with Et_2O:EtOH 4:1 (50.0 mL), and then left under stirring at room temperature overnight. Solid H_3L (0.0570 g, 0.313 mmol) was added, and the slightly darker mixture was stirred for 2 h. White NaCl was filtered off and discarded, while the solution was allowed to slowly evaporate to a final volume of 5 mL. The resulting orange precipitate was collected by filtration, washed quickly with ethanol (1 mL), and dried in vacuo (0.151 mg, 75.3%). Anal. Calcd for $C_{68}H_{82}F_{18}Fe_4O_{18}$ (1752.72): C, 46.60; H, 4.72; Fe, 12.74. Found: C, 46.47; H, 4.75; Fe, 13.42.[16] IR (KBr): 2972 ($\nu_{C-H,tBu}$), 2864 ($\nu_{C-H,pta}$), 1623, 1596 ($\nu_{C=O}$), 1447 ($\nu_{C=C,Ph}$), 1309, 1253, 1197, 1148 (ν_{C-F}), 1082 (ν_{C-O}) cm^{-1}. ^{1}H NMR (benzene-d_6, 298 K, 200 MHz): δ −24.5 (very br, 6H, $CH_{methine}$), 0.6 (br, 4H, *o*-H_{Ph}), 3.9 (br, 2H, *p*-H_{Ph}), 10.7 (br, 54H, ^{t}Bu), 12.3 (shoulder, 4H, *m*-H_{Ph}). MS-MALDI ToF (CH_3CN): *m*/*z* (with matrix) 1792.1494 ($[M + K]^+$, 40%), 1775.1685 ($[M + Na]^+$, 100), 1557.1079 ($[M − (pta)]^+$, 20); *m*/*z* (without matrix) 1792.1399 ($[M + K]^+$, 75%), 1775.1833 ($[M + Na]^+$, 70), 1557.1193 ($[M − (pta)]^+$, 65), 1362.0481 ($[M − (pta)_2]^+$, 100), 1127.0405 ($[M − Fe(L)(pta)_2]^+$, 70).

X-ray Crystallography. Single-crystal X-ray diffraction study was carried out on **1** with a four-circle Bruker X8-APEX diffractometer equipped with a Mo Kα generator (λ = 0.71073 Å), an area detector, and a Kryo-Flex cryostat and controlled by Bruker-Nonius X8APEX software. Crystal structure data: $C_{36}H_{50}F_{12}Fe_2O_{10}$, M_r = 982.46, crystal dimensions 0.42 × 0.35 × 0.24 mm^3, triclinic, space group $P\bar{1}$ (no. 2), a = 8.7808(4) Å, b = 10.5584(4) Å, c = 13.6098(6) Å, α = 67.7850(14)°, β = 89.1974(15)°, γ = 80.9034(15)°, V = 1151.98(9) $Å^3$, Z = 1, ρ_{calcd} = 1.416 g cm^{-3}, θ_{max} = 27.49°, T = 140(2) K, collected/independent reflections 23 381/5257, R(int) = 0.0260, final R indices R_1 = 0.0368, wR_2 = 0.0988 [$I > 2\sigma(I)$], R_1 = 0.0463, wR_2 = 0.1042 [all data], goodness-of-fit = 1.034. The structure was solved by direct methods using the SIR92[17] program and refined by full-matrix least-squares on F_o^2 using the SHELX-97[18] program with 294 parameters and 0 restraints; both programs are implemented in the WINGX[19] v1.80.05 package. The program Mercury 3.0.1[20] was used for graphics. All non-hydrogen atoms were refined anisotropically. Methine and CH_2 hydrogen atoms were located in ΔF maps and refined isotropically. The remaining methyl hydrogen atoms were added in idealized positions with torsion angle refinement (AFIX 137 card in SHELX-97) and with isotropic displacement parameters constrained to those of the attached carbon atoms. CCDC 912864 contains the supplementary crystallographic data for this paper. These data can be obtained free of charge from the Cambridge Crystallographic Data Centre via www.ccdc.cam.ac.uk/data_request/cif.

Magnetic Measurements. Direct current (dc) magnetic data were recorded using a Quantum Design MPMS SQUID magnetometer. Magnetic susceptibilities were measured on a 12.55 mg powder sample of **2** packed in a Teflon pellet with applied fields of 1 kOe from 1.9 to 30 K and of 10 kOe from 30 to 260 K. Data reduction was carried out using 1752.72 as the molecular weight and -816.28×10^{-6} emu mol^{-1} as the diamagnetic contribution, estimated from the Pascal's constants.[21] Alternating current (ac) susceptibility was recorded on a Quantum Design PPMS susceptometer on the same sample of **2**, while the above-mentioned MPMS SQUID apparatus was employed for the evaporated film.

Thermal Evaporation. Thermal evaporation of compound **2** was obtained in a homemade molecular evaporator chamber, equipped with a quartz crucible; temperature was monitored by a K-type thermocouple inserted in the powder sample. The temperature of the crucible was ramped gently up to the sublimation temperature (440 K) that corresponds to a relevant increase in the pressure of the chamber (from 2×10^{-7} up to 6×10^{-7} mbar). The system was maintained at this temperature for 48 h, in order to obtain a thick film deposit on a Teflon tape and to perform the magnetic measurements with a minimal contribution from the substrate. The sample mass (0.20(1) mg) was measured directly, while the thickness of the film (1.5(1) μm) was estimated based on AFM scratching measurements. Thinner films suitable for X-ray photoelectron spectroscopy (XPS) and time of flight secondary ion mass spectrometry (ToF-SIMS) characterization were obtained by a 10 min deposition on a Au/mica substrate.

XPS Measurements. Experiments were carried out in a UHV chamber equipped with X-ray source (non monochromatized Al Kα source, 1486.6 eV) and hemispherical analyzer by VSW mounting a 16-channel detector. The X-ray source, mounted at 54.44° with respect to the analyzer, was operated at a power of 100 W (10 kV and 10 mA). XPS spectra were measured at normal emission with a fixed pass energy of 44 eV. All spectra were referenced to the $Au4f_{5/2}$ peak at 83.9 eV. The inelastic background in the spectra was subtracted by means of the Shirley method. Data analysis was based on a standard method for deconvolution using mixed Gaussian (G) and Lorentzian (L) line shapes (ratio G/L = 30) for each component in the spectrum. Elemental composition of the samples was then evaluated using a semiempirical approach; the integrated intensity of each component was corrected with the photoionization cross-section calculated for each atom,[22] neglecting the differences in photoelectron escape length as a function of the kinetic energy.

ToF-SIMS Measurements. A TRIFT III spectrometer (Physical Electronics, Chanhassen, MN) equipped with a gold liquid-metal primary ion source was employed for the ToF-SIMS analyses. Positive- and negative-ion spectra were acquired with a pulsed, bunched 22 keV Au^+ primary ion beam by rastering the ion beam over a 100 μm × 100 μm sample area and maintaining static SIMS conditions; only positive-ion spectra were considered as relevant. Positive-ion spectra were calibrated to CH_3^+ (*m*/*z* = 15.023), $C_2H_3^+$ (*m*/*z* = 27.023), and $C_3H_5^+$ (*m*/*z* = 41.039). Mass resolution ($m/\Delta m$) was up to 10^4, depending on the sample. Theoretical isotopic patterns for the most relevant signals were calculated with Molecular Weight Calculator 6.49 Program.[23]

dx.doi.org/10.1021/ic400037c | *Inorg. Chem.* 2013, 52, 5897−5905

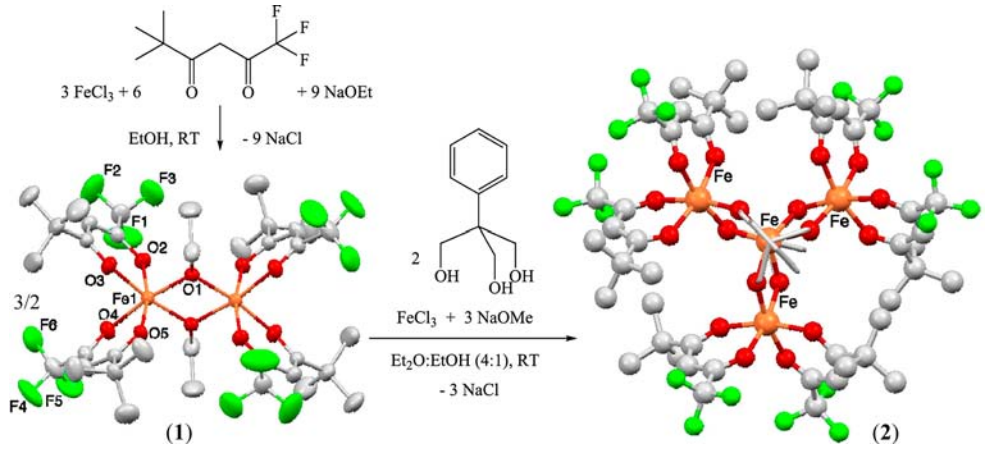

Figure 1. Synthetic reaction scheme for $[Fe_2(OEt)_2(pta)_4]$ (**1**) and $[Fe_4(L)_2(pta)_6]$ (**2**). Compound **1** is drawn from the X-ray molecular structure, viewed approximately along the *a* axis with ellipsoids at the 50% probability level (see Figure S3, Supporting Information, for further details). Compound **2** is drawn from the DFT-optimized structure of **Iso1** (see text) viewed along the idealized C_3 axis. Legend: Fe = orange, F = green, O = red, C = gray (hydrogen atoms omitted for clarity).

DFT Calculations. DFT-based structural optimizations were used to model compound **2** in the gas phase. Convergence criteria of 1.0×10^{-6} Hartree for SCF energy and 2.0×10^{-3} Hartree $Bohr^{-1}$ for the atomic forces were considered to get reliably converged structures. To solve the KS equations we applied the GPW formalism as implemented in the CP2K package.[24] Double-ζ basis set plus single polarization function was used to describe the MOs, and the augmented PW basis set was truncated to an energy of 400 Ry. GTH norm conserved PP were employed to describe the interaction between valence electrons and atomic cores. We used revPBE[25] with VdW corrections.[26] Optimizations were carried out on the $M_s = 5$ broken symmetry state. Single-point energy calculations were performed on optimized geometries with tighter SCF convergence criteria (5.0×10^{-7} Hartree) at the PBE0[27] level for the $S = 10$ and $M_s = 5$ spin states. The broken-symmetry approach was used to compute the exchange parameters.[28] A cubic cell with 25 Å side length was used throughout. To check the accuracy of the approach, we determined the optimized geometry and the exchange parameters in complex $[Fe_4(L)_2(dpm)_6]$.[5] Compared with the observed molecular structure, a maximum error of 2.5% resulted in the main geometrical parameters. The calculated value of the helical pitch, evaluated as the average dihedral angle between the FeO_2Fe and Fe_4 planes,[8a] was 71.1° (exp 68.8°). The computed nearest-neighbor exchange constant $J = 14.44$ cm^{-1} (as defined in eq 2) was also very close to the experimental value ($J = 16.37(12)$ cm^{-1}). Such results confirm the reliability of our computational protocol.

RESULTS AND DISCUSSION

Synthesis and Solution Studies. Treatment of bis(methoxido)-bridged dimers $[M_2(OMe)_2(dpm)_4]$ with stoichiometric amounts of $M'Cl_3$ and NaOMe and an excess of a tripodal ligand affords tetranuclear complexes $[Fe_4(L)_2(dpm)_6]$ (M = M′ = Fe),[5] $[CrFe_3(L)_2(dpm)_6]$ (M = Fe, M′ = Cr),[29] and $[Ga_4(L)_2(dpm)_6]$ (M = M′ = Ga).[29] In the case of tetrairon(III) complexes, reaction is conveniently carried out in two steps with isolation of the intermediate $[Fe_4(OMe)_6(dpm)_6]$.[5] Extension of this procedure to H*pta* complexes proved to be rather challenging, as they exhibit a much higher solubility in organic solvents and are difficult to isolate as pure solid phases. For instance, reaction between $FeCl_3$, H*pta*, and NaOMe in methanol failed to afford solid precursor $[Fe_2(OMe)_2(pta)_4]$, although in the same conditions the corresponding *dpm* complex precipitates out of the reaction mixture in 82% yield.[5] Concentration of the solution is also not useful, as it leads to coprecipitation of the desired diiron(III) complex and NaCl. We found that a very convenient variant to the procedure is replacement of methanol with ethanol. Following reaction of $FeCl_3$ with H*pta* and sodium ethoxide in ethanol (see Figure 1), NaCl precipitates and can be filtered off, while slow evaporation of the mother solution yields orange X-ray-quality crystals of bis(ethoxido)-bridged dimer $[Fe_2(OEt)_2(pta)_4]$ (**1**) in excellent yields. The tetranuclear compound $[Fe_4(L)_2(pta)_6]$ (**2**) was then assembled in solution from **1**, $FeCl_3$, and excess H_3L in a moderately polar medium (Et_2O:EtOH ≅ 4:1) and isolated in the solid state by slow evaporation of the filtered reaction mixture (see Figure 1).

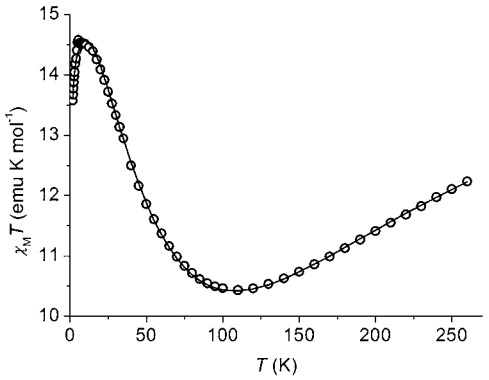

Figure 2. Temperature dependence of the $\chi_M T$ product for $[Fe_4(L)_2(pta)_6]$ (**2**). Solid curve has been calculated using the best-fit parameters reported in the text.

The fluorinated *pta* ligands convey to **2** a high solubility in most organic solvents. Furthermore, the two different substituents (CF_3 and ^{t}Bu) potentially lead to a mixture of geometrical isomers (vide infra), and we have so far been unable to obtain crystals of **2** suitable for X-ray diffraction. Infrared, ^{1}H NMR, and MS-MALDI ToF data, however, provide compelling evidence of compound structure.

In their infrared spectra, both **1** and **2** present C−F stretching bands in the 1310−1150 cm^{-1} range and the C═O bands of the coordinated *pta* ligands around 1600 cm^{-1}. Tetranuclear **2** is also characterized by a broad band of medium intensity at 1447 cm^{-1}, attributable to the aromatic C═C stretching. Furthermore, stretching of the $C-O_{alkoxide}$ bonds

dx.doi.org/10.1021/ic400037c | Inorg. Chem. 2013, 52, 5897−5905

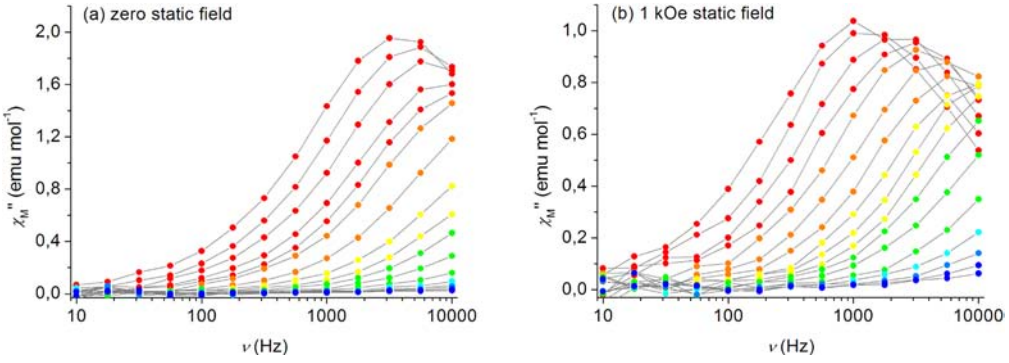

Figure 3. Imaginary component of the molar ac susceptibility, χ_M'', of **2** measured at (a) zero and (b) 1 kOe static fields in the 10−10 000 Hz frequency range from 1.9 (red) to 5.5 K (blue).

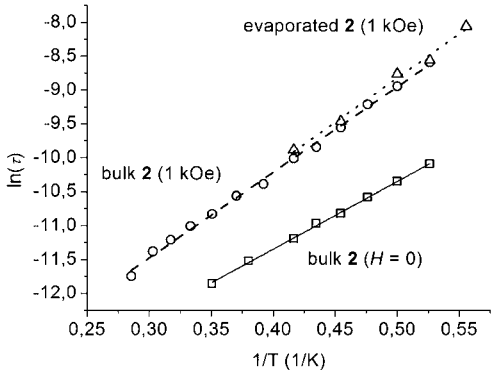

Figure 4. Arrhenius plots of $\ln(\tau)$ vs $1/T$ for compound **2** obtained from ac susceptibility measurements on a bulk sample in zero (□) and 1 kOe (○) static fields together with the data obtained on the evaporated sample on Teflon with a 1 kOe applied field (△).

diagnostically shifts from 1039 cm^{-1} in **1** to 1082 in **2** (see Figure S1, Supporting Information).

The room-temperature ^{1}H NMR spectrum of compound **2** in benzene-d_6 is dominated by broad, paramagnetically shifted resonances at 10.7 and −24.5 ppm attributable to ^{t}Bu and methine protons, respectively.[5] Weaker and broad signals at 0.6, 3.9, and 12.3 ppm are also present and can be assigned to phenyl protons (see Figure S2, Supporting Information). In fact, signals with similar chemical shifts (0.7, 4.0, and 12.1 ppm) are detected in the ^{1}H NMR spectrum of $[Fe_4(L)_2(dpm\text{-}d_{18})_6]$ featuring deuterated ^{t}Bu groups.[5] Consistent with the proposed assignment, addition of 1.5 equiv of H*pta* to a solution of $[Fe_4(L)_2(dpm\text{-}d_{18})_6]$ leads to the appearance of new narrow peaks at 17.1 (OH) and 5.80 (methine) ppm due to protons of H*dpm*-d_{18} in the enolic form and a broad signal at 9.9 ppm

Table 1. Summary of the Most Relevant Peaks Detected in the Positive-Ion ToF-SIMS Spectra of Drop-Cast and Evaporated Deposits of 2

experimental (*m*/*z*)			
drop cast	evaporated	theoretical (*m*/*z*)	assignment
1752.3 (weak)	1752.2 (medium)	1752.3	$[M]^+$
1557.2 (strong)	1557.0 (strong)	1557.2	$[M-(pta)]^+$
1362.1 (strong)	1362.0 (strong)	1362.1	$[M-(pta)_2]^+$
1127.1 (strong)	1127.0 (medium)	1127.1	$[M-Fe(L)(pta)_2]^+$

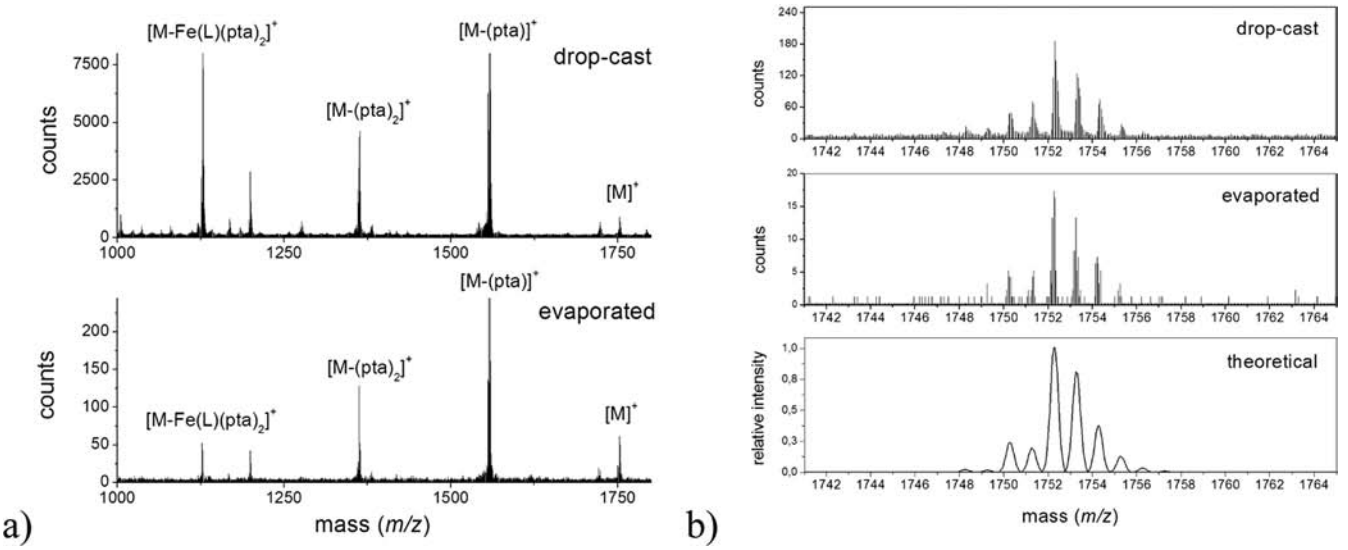

Figure 5. Positive-ion ToF-SIMS spectra of **2**: (a) comparison between evaporated and drop-cast deposits on gold; (b) expanded view of the molecular $[M]^+$ peaks together with the theoretical isotopic pattern.

dx.doi.org/10.1021/ic400037c | Inorg. Chem. 2013, 52, 5897−5905

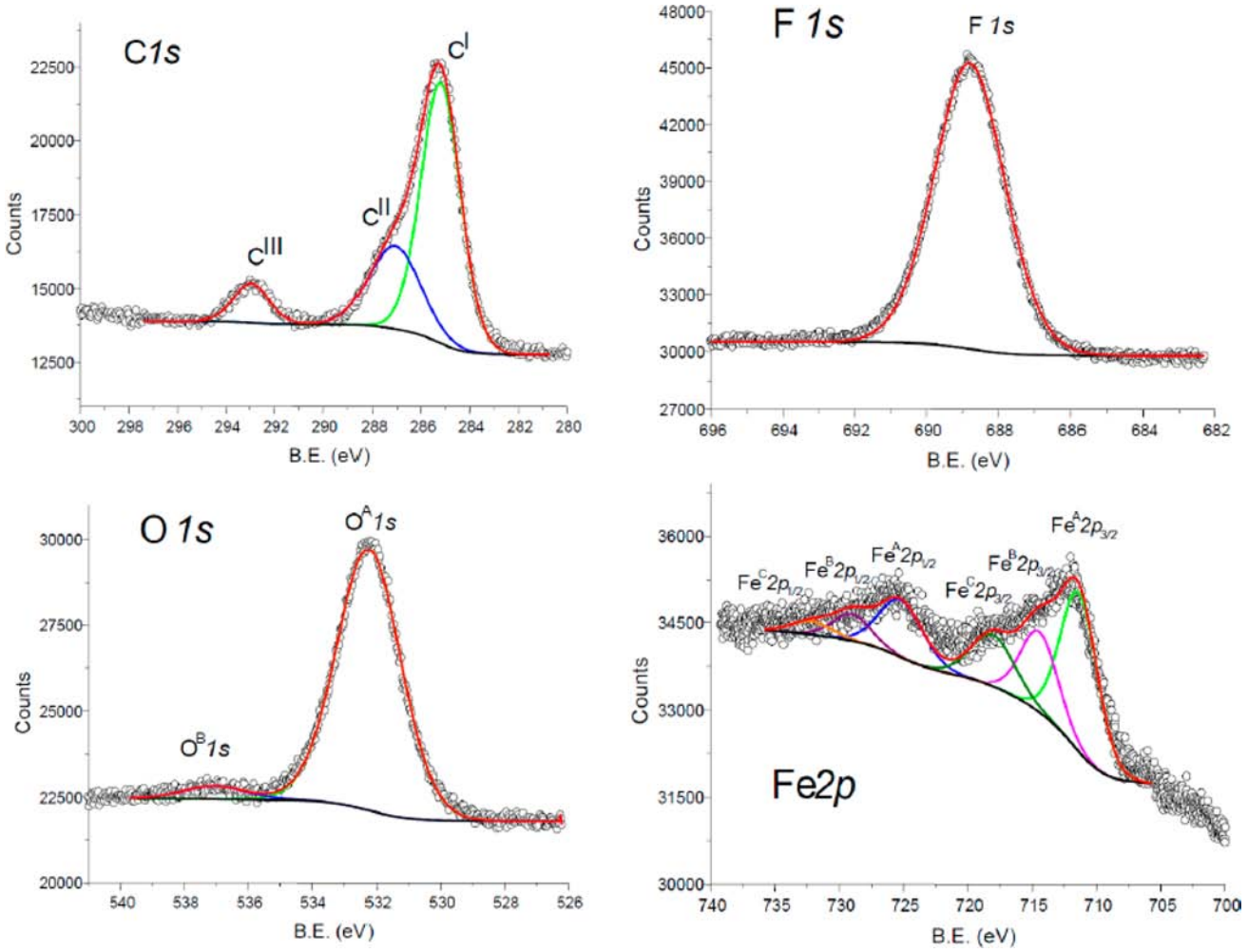

Figure 6. XPS spectra in the C1s, O1s, F1s, and Fe2p zones. Open circles indicate the experimental data and red line the resulting fit obtained from the sum of the different components (see text).

Table 2. Experimental (XPS) and Calculated Atomic Compositions of an Evaporated Deposit of 2[a]

element	Fe	F	O	C (C^I, C^{II}, C^{III})
expected (%)	3.7	16.7	16.7	63.0 (64.8, 26.6, 8.7)
experimental (%)	3.5	18.9	15.1	62.4 (64.8, 26.5, 8.7)

[a] C^I, C^{II}, and C^{III} indicate the aliphatic/aromatic, carbonyl/alcoholic, and fluorinated carbon contents, respectively, relative to the total carbon.

from ^{t}Bu protons of iron(III)-bound *pta* ligands. Concomitantly, the signals of free H*pta* at 15 (broad), 5.88, and 0.83 ppm (OH, methine, and ^{t}Bu protons, respectively) progressively decrease in intensity and disappear after 4 h, as expected from a ligand-exchange reaction on the preformed tetrairon(III) core

$$[Fe_4(L)_2(dpm\text{-}d_{18})_6] + x\text{H}pta \rightarrow [Fe_4(L)_2(dpm\text{-}d_{18})_{6-x}(pta)_x] + x\text{H}dpm\text{-}d_{18} \quad (1)$$

For comparison, in the same conditions $[Fe_4(L)_2(dpm)_6]$ exhibits resonances at 10.5 and −15.0 ppm, respectively.[5] The occurrence of larger paramagnetic shifts in iron(III) complexes of *pta* with respect to *dpm* was noted previously in the simpler compounds $[Fe(dpm)_3]$ and $[Fe(pta)_3]$, whose ^{t}Bu (methine) protons resonate at 12.9 (−28) and 14.7 (−40) ppm in $CDCl_3$ at 295 K.[30] A similar enhancement of spin delocalization by CF_3 substituents is found in the series $[Fe(acac)_3]$, $[Fe(tfac)_3]$, and $[Fe(hfac)_3]$ (H*acac* = acetylacetone; H*tfac* = 1,1,1-trifluoroacetylacetone; H*hfac* = 1,1,1,5,5,5-hexafluoroacetylacetone).[30] Finally, in the ^{1}H NMR spectra of **1**, for which one expects a decreased unpaired spin density on the *pta* ligands,[5] the signals from ^{t}Bu and methine protons exhibit a smaller paramagnetic shift and resonate at 9.5 and −20.0 ppm, respectively.

The MALDI-ToF mass spectrum of **2** in CH_3CN solution shows the molecular peaks $[M + K]^+$ and $[M + Na]^+$ at m/z = 1792 and 1775 and specific fragmentation clusters due to loss of *pta* ligands, iron ions, and tripodal ligands (see Experimental Section). The same pattern can be observed in the mass spectrum of the compound $[Fe_4(L)_2(dpm)_6]$, recorded in the same conditions,[31] thus further confirming that the two complexes are strictly isostructural.

In support to the reported experimental data, we performed DFT-based geometrical optimizations for three of the possible geometrical isomers of compound **2**. Two of them (**Iso1** and **Iso2**) are the only isomers with D_3 symmetry (neglecting the Ph substituent) and differ in the arrangement of ^{t}Bu and CF_3 groups. In **Iso1** and **Iso2**, the oxygen donors closer to CF_3 groups occupy cis and trans positions, respectively, in the coordination sphere of peripheral iron(III) ions (see Figure 1).

dx.doi.org/10.1021/ic400037c | Inorg. Chem. 2013, 52, 5897−5905

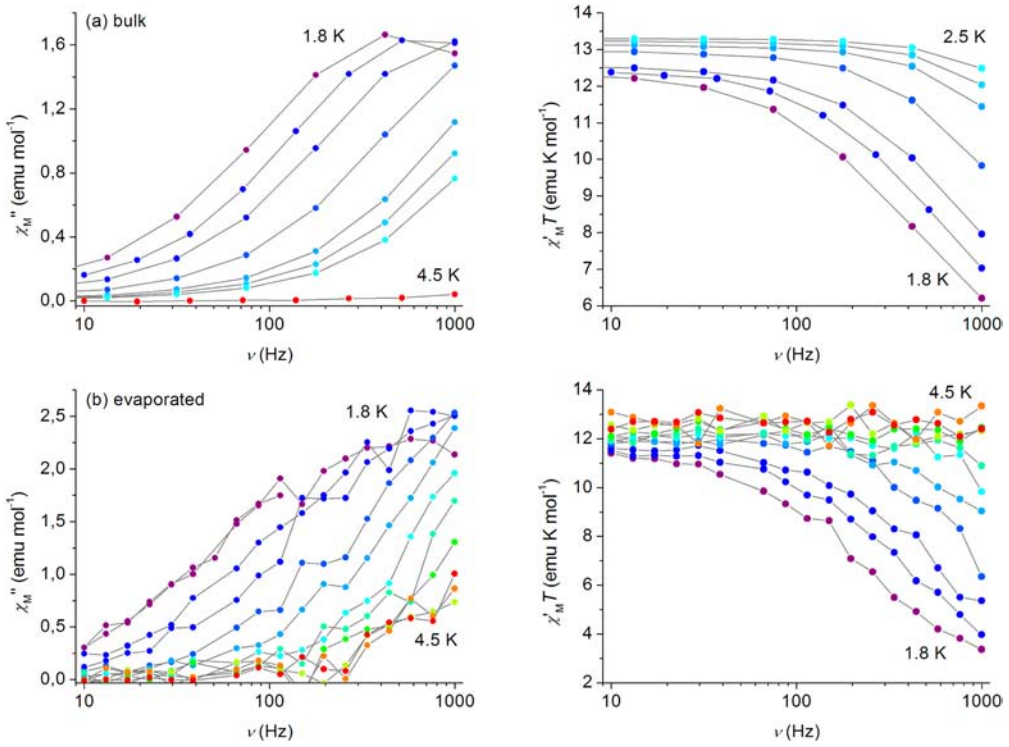

Figure 7. Frequency dependence of the out-of-phase component of the ac susceptibility χ_M'' (left) together with the $\chi_M'T$ product (right) measured for (a) bulk and (b) evaporated samples of **2** at 1 kOe static field and in the temperature range 1.8−4.5 K.

In the third isomer, **Iso3**, a mixed arrangement of ^{t}Bu and CF_3 groups was chosen as an example of a lower symmetry configuration (Figure S3, Supporting Information). From these calculations, we found that the three isomers are geometrically very similar to each other and to complex $[Fe_4(L)_2(dpm)_6]$ (see Table S1, Supporting Information). In particular, the computed helical pitches of 69.3°, 67.7°, and 70.5° are typical for this class of compounds.[8a] Turning now to the computed total energies, if **Iso1** is taken as energy reference, **Iso2** and **Iso3** are less stable by only 0.60 and 0.82 kcal mol^{-1}, respectively. If a nearly constant entropy contribution is assumed, from the computed total energies it can be inferred that the three isomers are quasi degenerate. A mixture of geometrical isomers is therefore expected, thus offering a possible explanation to the difficulties encountered in the isolation of X-ray quality crystals of **2**.

Crystal and Molecular Structure of $[Fe_2(OEt)_2(pta)_4]$ (1). Crystals of compound **1** suitable for X-ray diffraction were obtained directly by slow evaporation of the reaction mixture. Selected geometrical parameters at 140(2) K are reported in Table S2, Supporting Information, and the molecular structure is shown in Figure 1 and Figure S4, Supporting Information. Crystals are triclinic, and the asymmetric unit comprises a half-dimer molecule. The two iron(III) ions are related by an inversion center and bridged by two ethoxido groups. Oxygen donors of these two groups in cis position and two bidentate *pta* ligands occupy the six coordination sites around the metal atoms, giving rise to a distorted octahedral geometry. The two iron−ethoxido bond distances are slightly asymmetric (Fe−O1 = 1.9497(13) and Fe−O1^i = 1.9706(13) Å, ^{i} = $-x$, $-y$, $-z$). These and all other coordination bond distances agree well with those reported in the literature for similar dimer compounds.[32] The four carbon−oxygen bonds within the *pta* ligands are all very similar with an average distance of 1.259(2) Å, only slightly elongated with respect a typical C=O double bond in carbonyl compounds. Asymmetric substitution of the *β*-diketonato ligands (electron-donor ^{t}Bu group against electron-withdrawing CF_3 fragment) is reflected in the different C−C bond distances within the chelate rings (1.365(3) and 1.379(3) Å for the C−C bond close to CF_3 and 1.404(3) and 1.418(3) Å for the C−C close to ^{t}Bu). Such asymmetry is either not present or less pronounced in symmetrically substituted ligands.[32]

Direct Current Magnetic Studies. The temperature dependence of the molar magnetic susceptibility, χ_M, in low fields (1−10 kOe) for compound **2** was measured between 1.9 and 260 K, and data are reported in Figure 2 as a χ_MT vs T plot. The behavior of the χ_MT curve is characteristic of Fe_4 systems, where the dominant antiferromagnetic interaction between the central and the peripheral high-spin iron(III) centers generates an S = 5 ground state.[5,6,8,9,33] The curve shows a value of 12.25 emu K mol^{-1} at 260 K, lower than expected for four uncoupled iron(III) ions (17.51 emu K mol^{-1} with g = 2.00); then it features an initial decrease upon cooling, reaching a minimum at around 105 K (10.10 emu K mol^{-1}). Upon further cooling, the χ_MT product increases again up to 14.52 emu K mol^{-1} at 9 K, in agreement with selective population of an S = 5 ground state (expected value 15.00 emu K mol^{-1} with g = 2.00). The final drop at very low T presumably arises from magnetic saturation, anisotropy effects, or intermolecular interactions.

In order to evaluate the magnetic exchange interactions among the four iron(III) centers, data have been analyzed using a Heisenberg *plus* Zeeman spin Hamiltonian, assuming a 3-fold molecular symmetry

$$\hat{\mathcal{H}} = J(\hat{\mathbf{S}}_1\cdot\hat{\mathbf{S}}_2 + \hat{\mathbf{S}}_1\cdot\hat{\mathbf{S}}_3 + \hat{\mathbf{S}}_1\cdot\hat{\mathbf{S}}_4) + J'(\hat{\mathbf{S}}_2\cdot\hat{\mathbf{S}}_3 + \hat{\mathbf{S}}_3\cdot\hat{\mathbf{S}}_4 + \hat{\mathbf{S}}_2\cdot\hat{\mathbf{S}}_4) + g\mu_B\hat{\mathbf{S}}\cdot\hat{\mathbf{H}} \quad (2)$$

dx.doi.org/10.1021/ic400037c | Inorg. Chem. 2013, 52, 5897−5905

where $\mathbf{S}_1$ is the spin vector for the central iron ion, $\mathbf{S}_2$, $\mathbf{S}_3$, and $\mathbf{S}_4$ are the spin vectors for the peripheral centers, $\mathbf{S}$ is the total spin vector, $\mathbf{H}$ is the applied magnetic field, and J and J' are the nearest-neighbor (n.n.) and the next-nearest neighbor (n.n.n.) exchange coupling constants, respectively. The drop of the $\chi_M T$ curve below 5 K was phenomenologically reproduced by introducing a Curie−Weiss correction θ to the susceptibility calculated from eq 2, i.e., $\chi_M^{corr} = \chi_M T\ (T - \theta)^{-1}$.[33] Quantitative fitting of the data yielded the following parameters: g = 1.9900(13), J = 16.20(6) cm^{-1}, J' = 0.53(4) cm^{-1}, θ = −0.173(19) K. The coupling constant J is antiferromagnetic, as expected, fully reflecting the value found in compounds of this family.[5,6,8,9] DFT broken-symmetry calculations correctly predict S = 5 as the ground state with computed J values of 12.62, 9.85, and 8.61 cm^{-1} for **Iso1**, **Iso2**, and **Iso3**, respectively (using J convention in the Hamiltonian, as in eq 2). Notice that among the three isomers considered **Iso1** has both the lowest energy and the calculated J value in closest agreement with experiment.

A small but significant antiferromagnetic constant J' is also experimentally required in order to give an accurate fit. In other Fe_4 complexes, n.n.n. exchange interactions are found to be also small but either ferro- or antiferromagnetic.[5,6,8,9] As the J' parameter is likely to compensate for systematic errors in the measurement and data treatment (e.g., inaccuracy in diamagnetic correction, neglection of temperature-independent paramagnetism, departures from 3-fold symmetry) the real nature of n.n.n. interactions in Fe_4 complexes remains to be fully ascertained.

Alternating Current Magnetic Studies. Simple paramagnets do not show any imaginary (out-of-phase) component χ'' of the complex susceptibility in zero static field, while SMMs are characterized by freezing of the magnetization at low temperature and appearance of a nonzero, frequency-dependent out-of-phase response. The magnetization dynamics of compound **2** was then investigated by ac susceptibility measurements in zero and 1 kOe static fields. Analysis was performed as a function of both temperature (down to 1.9 K) and frequency of the oscillating field (ν = 10−10 000 Hz), and results are reported in Figure 3. In both zero and 1 kOe static fields, compound **2** shows a frequency dependence of the maxima in the χ'' vs T plots and therefore behaves as a SMM.

Within the Debye model[34] commonly employed to analyze the ac response of SMMs, a maximum in χ'' is observed when the relaxation time τ equals $(2\pi\nu)^{-1}$. The frequency dependence of the out-of-phase susceptibility at constant temperature was here fitted using the so-called extended Debye model, which accounts for a distribution of relaxation times through the width parameter α

$$\chi''(\omega) = (\chi_T - \chi_S)\frac{(\omega\tau)^{1-\alpha}\cos(\alpha\pi/2)}{1 + 2(\omega\tau)^{1-\alpha}\sin(\alpha\pi/2) + (\omega\tau)^{2-2\alpha}} \quad (3)$$

In the above equation, $\omega = 2\pi\nu$ and χ_T and χ_S are the isothermal and adiabatic susceptibilities, that is, the susceptibilities observed in the two limiting cases $\nu \to 0$ and $\nu \to \infty$, respectively. The model is satisfactory and affords α values, which at the lowest temperatures approach 0.25 and 0.30 in zero and 1 kOe static fields, respectively, and decrease toward 0 upon heating.

Relaxation times τ obtained from this analysis are shown in an Arrhenius plot in Figure 4 along with data for the evaporated compound (see below). The linear $\ln(\tau)$ vs $1/T$ plots indicate a thermally activated relaxation mechanism in the explored temperature range, as described by the Arrhenius law, $\tau = \tau_0 \exp(U_{eff}/k_B T)$. The best-fit parameters U_{eff}/k_B and τ_0 are 9.9(1) K and 2.3(1) 10^{-7} s in zero static field and 13.0(2) K and 2.0(2) 10^{-7} s at 1 kOe. The smaller effective barrier at H = 0 is presumably indicative of efficient resonant tunneling processes, which are substantially reduced by application of an external field.

Sublimation in High-Vacuum Conditions. Sublimation of compound **2** was performed in a HV (10^{-7} mbar) chamber. Molecule sublimation started at the temperature of (440 ± 5) K, with an increase of the chamber pressure from 2 × 10^{-7} to 6 × 10^{-7} mbar. For comparison $[Fe_4(L)_2(dpm)_6]$ evaporates at (500 ± 10) K in the same experimental conditions. In order to determine whether **2** undergoes any degradation upon sublimation, thin films were deposited on a Au/mica substrate and chemically characterized by ToF-SIMS and XPS.

In Figure 5a the positive-ion ToF-SIMS spectrum of the evaporated compound is compared with that of a drop-cast deposit on gold, obtained from a diluted solution of **2** in dichloromethane. Fragmentation patterns of the two samples are practically identical. The $[M]^+$ molecular ion peak of medium intensity at m/z = 1752.2 is present in both spectra, and its isotopic pattern is in perfect agreement with that predicted for an intact Fe_4 molecule (Figure 5b). Additional peaks are detected in both drop-cast and evaporated samples, the strongest ones being attributed to $[M-(pta)]^+$, $[M-(pta)_2]^+$, and $[M-Fe(L)(pta)_2]^+$ fragments, as detailed in Table 1. Overall, the fragmentation pattern bears strong resemblance with that observed in other Fe_4 systems by ToF-SIMS[35] and in **2** itself by MALDI-ToF mass spectrometry (see Experimental Section).

The results of our ToF-SIMS investigation suggest that molecules of **2** remain chemically intact upon evaporation. This evidence is supported by the semiquantitative XPS analysis performed on the evaporated film grown on a Au/mica substrate (Figure 6). In the C1s zone, three contributions are clearly distinguishable: a principal peak due to the aliphatic and aromatic carbon atoms at 285.2 eV (C^I), a shoulder due to the carbonyl and alcoholic carbon atoms at 287.0 eV (C^{II}), and a well-separated component at 292.9 eV (C^{III}) attributable to the carbon atoms of CF_3 groups. As reported in Table 2, the relative intensities of these contributions are very close to the expectation for intact **2**.

In the O1s and F1s regions, only single contributions can be distinguished at 532.2 and 688.6 eV, respectively (excluding a small contribution due to the oxygen shakeup at 537.0 eV). The Fe2p region shows a typical structured signal with a principal contribution at 711.5 eV due to the $Fe2p_{3/2}$ component of oxidized iron; this binding energy and the presence of a shakeup satellite peak at 718.3 eV confirm the presence of Fe^{III} species.[36] In addition to the $Fe2p_{1/2}$ component at 725.5 eV and its small satellite at 732.1 eV, two additional components at 714.7 and 729.2 eV were included in the fit to optimize analysis. Table 2 shows the good agreement between the experimental and calculated atomic compositions. Notice that the CF_3 groups act as useful chemical markers for XPS studies thanks to their well-resolved C1s component and the presence of fluorine atoms.

Since chemical integrity is not a sufficient condition for retention of SMM features, a thick film of compound **2** was deposited on Teflon and its ac susceptibility measured in the

dx.doi.org/10.1021/ic400037c | Inorg. Chem. 2013, 52, 5897−5905

frequency range (10−1000 Hz) available in the more sensitive SQUID susceptometer (Figure 7). Maxima are barely visible only at the lowest temperatures explored, but a behavior well comparable with that of the pristine compound can be unambiguously observed. In spite of the higher signal-to-noise ratio, data treatment using the Debye model (eq 3) afforded a linear Arrhenius plot with τ_0 = 1.6(9) 10^{-7} s and U_{eff}/k_B = 14(1) K (Figure 4). Activation parameters are within the experimental error from those of the bulk material, providing conclusive evidence that fluorinated compound **2** fully retains its molecular structure and SMM behavior upon sublimation. Noticeably, evaporated samples of $[Fe_4(L)_2(dpm)_6]$ exhibit a distinctly lower barrier than the bulk crystalline material (12.2 vs 15.6 K),[5,13a] pointing to more pronounced differences between the two solid phases.

CONCLUSIONS

In this work, we replaced *dpm* ligands in complex $[Fe_4(L)_2(dpm)_6]$ with partially fluorinated *β*-diketonates (*pta*) in order to enhance volatility with retention of SMM behavior. Combined ToF-SIMS, XPS, and ac susceptibility measurements provide clear evidence that the chemical structure and magnetic properties of $[Fe_4(L)_2(pta)_6]$ (**2**) remain unvaried upon thermal evaporation, which is effectively carried out at temperatures as low as (440 ± 5) K for pressures around 10^{-7} mbar. This new fluorinated derivative represents the second example of an evaporable polynuclear SMM. At the same time, it provides an excellent starting point for design of new SMMs carrying specific surface-binding groups while exhibiting manageable sublimation temperatures.

ASSOCIATED CONTENT

Supporting Information

Infrared spectra as KBr disks of **1** and **2**, 200 MHz ^{1}H NMR spectrum of **2** at room temperature in benzene-d_6, DFT-optimized geometrical structures of **Iso1**−**3**, table of experimental and computed distances and angles for $[Fe_4(L)_2(dpm)_6]$, and computed data for **Iso1**−**3**, picture of the molecular structure of **2** together with atom-numbering scheme, table with selected experimental distances and angles for **1** (PDF); X-ray crystallographic file of **2** (CIF). This material is available free of charge via the Internet at http://pubs.acs.org.

AUTHOR INFORMATION

Corresponding Author

*E-mail: andrea.cornia@unimore.it (A.C.); roberta.sessoli@unifi.it (R.S.).

Notes

The authors declare no competing financial interest.

ACKNOWLEDGMENTS

We thank the European Research Council for funding through the Advanced Grant MolNanoMaS (no. 267746) and Italian MIUR for support through FIRB project "Nanomagneti molecolari su superfici metalliche e magnetiche per applicazioni nella spintronica molecolare" (RBAP117RWN).

REFERENCES

(1) (a) Gatteschi, D.; Sessoli, R.; Villain, J. *Molecular Nanomagnets*; Oxford University Press: New York, 2006. (b) Vincent, R.; Klyatskaya, S.; Ruben, M.; Wernsdorfer, W.; Balestro, F. *Nature* **2012**, *488*, 357−360.

(2) (a) Rinehart, J. D.; Fang, M.; Evans, W. J.; Long, J. R. *Nat. Chem.* **2011**, *3*, 538−542. (b) Rinehart, J. D.; Fang, M.; Evans, W. J.; Long, J. R. *J. Am. Chem. Soc.* **2011**, *133*, 14236−14239. (c) Blagg, R. J.; Muryn, C. A.; McInnes, E. J. L.; Tuna, F.; Winpenny, R. E. P. *Angew. Chem., Int. Ed.* **2011**, *50*, 6530−6533. (d) Millios, C. J.; Vinslava, A.; Wernsdorfer, W.; Moggach, S.; Parsons, S.; Perlepes, S. P.; Christou, G.; Brechin, E. K. *J. Am. Chem. Soc.* **2007**, *129*, 2754−2755.

(3) (a) Domingo, N.; Bellido, E.; Ruiz-Molina, D. *Chem. Soc. Rev.* **2012**, *41*, 258−302. (b) Cornia, A.; Mannini, M.; Sainctavit, P.; Sessoli, R. *Chem. Soc. Rev.* **2011**, *40*, 3076−3091.

(4) Kahle, S.; Deng, Z.; Malinowski, N.; Tonnoir, C.; Forment-Aliaga, A.; Thontasen, N.; Rinke, G.; Le, D.; Turkowski, V.; Rahman, T. S.; Rauschenbach, S.; Ternes, M.; Kern, K. *Nano Lett.* **2012**, *12*, 518−521.

(5) Accorsi, S.; Barra, A.-L.; Caneschi, A.; Chastanet, G.; Cornia, A.; Fabretti, A. C.; Gatteschi, D.; Mortalo, C.; Olivieri, E.; Parenti, F.; Rosa, P.; Sessoli, R.; Sorace, L.; Wensdorfer, W.; Zobbi, L. *J. Am. Chem. Soc.* **2006**, *128*, 4742−4755.

(6) Barra, A.-L.; Caneschi, A.; Cornia, A.; Fabrizi de Biani, F.; Gatteschi, D.; Sangregorio, C.; Sessoli, R.; Sorace, L. *J. Am. Chem. Soc.* **1999**, *121*, 5302−5310.

(7) Mannini, M.; Pineider, F.; Sainctavit, P.; Joly, L.; Fraile-Rodríguez, A.; Arrio, M.-A.; Cartier dit Moulin, C.; Wernsdorfer, W.; Cornia, A.; Gatteschi, D.; Sessoli, R. *Adv. Mater.* **2009**, *21*, 167−171.

(8) (a) Gregoli, L.; Danieli, C.; Barra, A.-L.; Neugebauer, P.; Pellegrino, G.; Poneti, G.; Sessoli, R.; Cornia, A. *Chem.—Eur. J.* **2009**, *15*, 6456−6467. (b) Barra, A.-L.; Bianchi, F.; Caneschi, A.; Cornia, A.; Gatteschi, D.; Gorini, L.; Gregoli, L.; Maffini, M.; Parenti, F.; Sessoli, R.; Sorace, L.; Talarico, A. M. *Eur. J. Inorg. Chem.* **2007**, 4145−4152. (c) Rodriguez-Douton, M. J.; Mannini, M.; Armelao, L.; Barra, A.-L.; Tancini, E.; Sessoli, R.; Cornia, A. *Chem. Commun.* **2011**, *47*, 1467−1469.

(9) (a) Rodriguez-Douton, M. J.; Cornia, A.; Sessoli, R.; Sorace, L.; Barra, A.-L. *Dalton Trans.* **2010**, *39*, 5851−5859. (b) Prasad, T. K.; Poneti, G.; Sorace, L.; Rodriguez-Douton, M. J.; Barra, A.-L.; Neugebauer, P.; Costantino, L.; Sessoli, R.; Cornia, A. *Dalton Trans.* **2012**, *41*, 8368−8378.

(10) Burzurí, E.; Zyazin, A. S.; Cornia, A.; van der Zant, H. S. J. *Phys. Rev. Lett.* **2012**, *109*, 147203.

(11) Mannini, M.; Pineider, F.; Sainctavit, Ph.; Danieli, C.; Otero, E.; Sciancalepore, C.; Talarico, A. M.; Arrio, M.-A.; Cornia, A.; Gatteschi, D.; Sessoli, R. *Nat. Mater.* **2009**, *8*, 194−197.

(12) Mannini, M.; Pineider, F.; Danieli, C.; Totti, F.; Sorace, L.; Sainctavit, Ph.; Arrio, M.-A.; Otero, E.; Joly, L.; Cesar, J. C.; Cornia, A.; Sessoli, R. *Nature* **2010**, *468*, 417−421.

(13) (a) Margheriti, L.; Mannini, M.; Sorace, L.; Gorini, L.; Gatteschi, D.; Chiappe, D.; Moroni, R.; Buatier de Mongeot, F.; Cornia, A.; Piras, F. M.; Magnani, A.; Sessoli, R. *Small* **2009**, *12*, 1460−1466. (b) Lodi Rizzini, A.; Krull, C.; Balashov, T.; Mugarza, A.; Nistor, C.; Sessi, V.; Klyatskaya, S.; Ruben, M.; Stepanow, S.; Gambardella, P. *Nano Lett.* **2012**, *12*, 5703−5707. (c) Yi, X.; Bernot, K.; Pointillart, F.; Poneti, G.; Calvez, G.; Daiguebonne, C.; Guillou, O.; Sessoli, R. *Chem.—Eur. J.* **2012**, *18*, 11379−11387.

(14) (a) Matsumura, D.; Yokoyama, T.; Amemiya, K.; Kitagawa, S.; Ohta, T. *Phys. Rev. B* **2002**, *66*, 024402. (b) Vollmer, R.; van Dijken, S.; Poelsema, B. *Phys. Rev. B* **1999**, *60*, 6277−6280.

(15) Viguier, R.; Serratrice, S.; Dupraz, A.; Dupuy, C. *Eur. J. Inorg. Chem.* **2001**, 1789−1795.

(16) Fe content was determined by complexometric titration with EDTA, see: Jeffery, J. H.; Bassett, J.; Mendham, J.; Denney, R. C. *Vogel's Textbook of Quantitative Chemical Analysis*, 5th ed.; Longman Group UK Limited, 1989; p 326 and following.

(17) (a) Altomare, A.; Cascarano, G.; Giacovazzo, C.; Guagliardi, A. *J. Appl. Crystallogr.* **1993**, *26*, 343−350. (b) Altomare, A.; Cascarano, G.; Giacovazzo, C.; Guagliardi, A.; Burla, M. C.; Polidori, G.; Camalli, M. *J. Appl. Crystallogr.* **1994**, *27*, 435−436.

(18) (a) Sheldrick, G. M. *SHELX97, Programs for Crystal Structure Analysis*; University of Göttingen: Göttingen, 1997. (b) Sheldrick, G. M. *Acta Crystallogr., Sect. A: Found. Crystallogr.* **2008**, *A64*, 112−122.
(19) Farrugia, L. J. *J. Appl. Crystallogr.* **1999**, *32*, 837−838.
(20) Macrae, C. F.; Bruno, I. J.; Chisholm, J. A.; Edgington, P. R.; McCabe, P.; Pidcock, E.; Rodriguez-Monge, L.; Taylor, R.; van de Streek, J.; Wood, P. A. *J. Appl. Crystallogr.* **2008**, *41*, 466−470.
(21) Bain, G. A.; Berry, J. F. *J. Chem. Educ.* **2008**, *85*, 532−536.
(22) (a) http://ulisse.elettra.trieste.it. (b) Yeh, J. J.; Lindau, I. *At. Data Nucl. Data Tables* **1985**, *32*, 1−155.
(23) http://omics.pnl.gov/software/MWCalculator.php.
(24) Mundy, C. J.; Mohamed, F.; Schiffman, F.; Tabacchi, G.; Forbert, H.; Kuo, W.; Hutter, J.; Krack, M.; Iannuzzi, M.; McGrath, M.; Guidon, M.; Kuehne, T. D.; Laino, T.; VandeVondele, J.; Weber, V. *CP2K software package*; http://cp2k.berlios.de.
(25) Zhang, Y. K.; Yang, W. T. *Phys. Rev. Lett.* **1998**, *80*, 890.
(26) Grimme, S.; Antony, J.; Ehrlich, S.; Krieg, H. *J. Chem. Phys.* **2010**, *132*, 154104.
(27) Ernzerhof, M.; Scuseria, G. E. *J. Chem. Phys.* **1999**, *110*, 5029−5036.
(28) (a) Noodleman, L.; Norman, J. G., Jr. *J. Chem. Phys.* **1979**, *70*, 4903−4906. (b) Noodleman, L. *J. Chem. Phys.* **1981**, *74*, 5737−5743. (c) Bencini, A.; Totti, F. *J. Chem. Theory Comput.* **2009**, *5*, 144−154 and references therein.
(29) Tancini, E.; Rodriguez-Douton, M. J.; Sorace, L.; Barra, A.-L.; Sessoli, R.; Cornia, A. *Chem.—Eur. J.* **2010**, *16*, 10482−10493.
(30) Kissler, K. D.; Sheppard, S. K.; Eaton, G. R.; Eaton, S. S. *J. Magn. Reson.* **1985**, *63*, 74−87.
(31) MS-MALDI ToF (CH_3CN) of $[Fe_4(L)_2(dpm)_6]$: *m*/*z* (with matrix) 1719.6819 ($[M + K]^+$, 100%), 1703.6969 ($[M + Na]^+$, 20), 1497.5466 ($[M - (dpm)]^+$, 15), 1314.3870 ($[M - (dpm)_2]^+$, 25), 1114.2723 ($[M - Fe(dpm)_3 + K]^+$, 100).
(32) Le Gall, F.; Fabrizi de Biani, F.; Caneschi, A.; Cinelli, P.; Cornia, A.; Fabretti, A. C.; Gatteschi, D. *Inorg. Chim. Acta* **1997**, *262*, 123−132 and references therein.
(33) O'Connor, C. J. *Prog. Inorg. Chem.* **1982**, *29*, 203−283.
(34) (a) Cole, K. S.; Cole, R. H. *J. Chem. Phys.* **1941**, *9*, 341−352. (b) Dekker, C.; Arts, A. F. M.; Wijn, H. W.; van Duyneveldt, A. J.; Mydosh, J. A. *Phys Rev. B* **1989**, *40*, 11243−11251.
(35) Pineider, F.; Mannini, M.; Danieli, C.; Armelao, L.; Piras, F. M.; Magnani, A.; Cornia, A.; Sessoli, R. *J. Mater. Chem.* **2010**, *20*, 187−194.
(36) (a) Yamashita, T.; Hayes, P. *Appl. Surf. Sci.* **2008**, *254*, 2441−2449. (b) Mekki, A.; Holland, D.; McConville, C. F.; Salim, M. *J. Non-Cryst. Solids* **1996**, *208*, 267−276.